Contemporary Mathematics
https://ojs.wiserpub.com/index.php/CM/

Research Article

Numerical Solution to the Cargo LeRoux Model

Ilyas Khan[1*], Sidrah Ahmed[2], Adnan Rauf[2], Wei Sin Koh[3]

[1] Department of Mathematics, College of Science Al-Zulfi, Majmaah University, Al-Majmaah, 11952, Saudi Arabia
[2] Department of Mathematics, Basic Sciences and Humanities, Sukkur IBA University, Sukkur, Pakistan
[3] INTI International University, Persiaran Perdana BBN Putra Nilai, Nilai, 71800, Malaysia
E-mail: i.said@mu.edu.sa

Received: 29 March 2025; **Revised:** 12 May 2025; **Accepted:** 5 June 2025

Abstract: This article presents the Godunov method applied to solve the Riemann problem for the isentropic Cargo LeRoux model. The pressure-density relation for this model yields Riemann invariants that are complicated and computationally challenging to process. Only the exact solution has been developed for this model, and no numerical method has been applied thus far. Incorporating many computational checks is necessary for the numerical simulations of this model. Hence, it is ensured that variables and related quantities in the pressure equation remain positive, and the integrals converge within given accuracy conditions without casting complex values. Two nonlinear equations are obtained for possible wave configurations in the exact solutions. This system of two nonlinear algebraic equations is solved with the Newton-Raphson method. This root-finding process is sensitive to the initial guess values. A special algorithm is used to guess the initial values for the Newton-Raphson procedure. It is based on evaluating the residual functions and finding appropriate initial guesses by sorting the answers. These steps effectively simulate complex terms. The system is hyperbolic, with three distinct eigenvalues of the Jacobian matrix, and the solution consists of three waves. The tests showed that the Godunov scheme is applicable and achieves good accuracy for this model. However, the central scheme fails to solve this problem. This study bridges the gap between model analysis and developing numerical methods for solving isentropic Euler equation models.

***Keywords*:** Riemann problem, isentropic Euler equations, Godunov methods, Cargo LeRoux model, Smart grid

MSC: 35L65, 35Q31, 65M08, 65M12, 76N10

1. Introduction

The Riemann problem involves discontinuous initial data coupled with a hyperbolic system of partial differential equations. It has been developed as one of the key tools for studying the nature of complex phenomena in various fields, including multi-phase flows, magnetogasdynamics, astrophysics, and geophysical flows [1–6]. Researchers are still developing exact and numerical solutions for the Riemann problem using various approaches. Several recent studies have examined the Riemann problem in the context of the Cargo-LeRoux model, including works on wave interactions, symmetry methods, and pressure perturbations (see [7–10]). Similar work includes the Riemann problem for an ideal polytropic dusty gas [11], the study of weak shock waves for the drift-flux model of compressible two-phase flow by Kuila

Copyright ©2026 Ilyas Khan, et al.
DOI: https://doi.org/10.37256/cm.7120266876
This is an open-access article distributed under a CC BY license
(Creative Commons Attribution 4.0 International License)
https://creativecommons.org/licenses/by/4.0/

and Raja Sekhar [12], the Riemann problem solution for compressible duct flow [13], the exact solution for relativistic magnetohydrodynamics in [14] and solution for one-dimensional inviscid and isentropic flow of a mixture of a non-ideal gas with small solid particles developed in [15].

Numerous numerical techniques have been developed to simulate hyperbolic systems encountered in various fields. These areas include fluid mechanics, astrophysics, black holes, the oil industry, aerodynamics, cancer modelling, magnetohydrodynamics, and filtration theory. However, the isentropic Euler equations and related models have been primarily investigated using exact solvers in recent years. For example, Li in [16] presented the Riemann solution to the isentropic Euler equation in a scenario where the temperature drops to zero. This work was extended to vanishing pressure limits by Chen and Liu [17]. The polytropic gas flow has been studied by Yin et al. [18], and the isentropic magnetogasdynamics model has been studied by Shen [19]. The Riemann solutions for the isothermal van der Waals dusty gas model have been investigated recently [20]. Many of these models are related to phenomena involving volcanic and cosmic explosions, supersonic flight in polluted air, and engineering science problems.

The purpose of this paper is twofold. The first task is revisiting the solution derived in [10]. Additional details about the solution profile within the rarefaction waves that were previously omitted have been included. A review of the exact solution is necessary before discussing the Godunov method for this model. This review offers a comprehensive and accurate solution, encompassing all aspects of the solution. Moreover, this review is essential because it shows the complexity of numerical calculations involved in applying numerical methods. The second task is to provide a detailed numerical scheme and accompanying numerical results. This work represents the first step toward numerical simulations of the isentropic Cargo-LeRoux model. It is a continuation of the applications of the Godunov method, which have already been applied to many models [21–29]. This numerical study can help evaluate various numerical methods since its construction relies on a locally exact solver.

This paper is composed of four sections. Section 1 summarizes the work on Riemann problems related to the context. Section 2 reviews exact solutions for the model under consideration. Section 3 briefly outlines the working steps of the numerical scheme, and section 4 presents numerical results, followed by a conclusion.

2. Cargo LeRoux model and associated Riemann problem

The recent work in [10] has motivated us to undertake this research. Sumita and Sahadeb introduced the Cargo LeRoux model as a system of partial differential equations given below:

$$\begin{aligned}
&\rho_t + (\rho u)_x = 0 \\
&(\rho q)_t + (\rho q u)_x = 0 \\
&(\rho u)_t + \left(\rho u^2 + p + q\right)_x = 0 \\
&(\rho e - q)_t + ((\rho u + p)u)_x = 0.
\end{aligned} \tag{1}$$

The independent variables are x and t, representing one-dimensional space and time, respectively. The dependent variables are ρ, q, u, p, and e, which denote density, potential, velocity, pressure, and total energy, respectively. Partial derivatives are denoted by conventional x and t subscripts. This model has been modified for the case of the van der Waals gas flux perturbation pressure equation of state. As a result, the pressure density relationship becomes $p = A\rho/(1-a\rho)^{\gamma}$. Here γ is an adiabatic constant that controls the sensitivity response of density variations to pressure. The constant A appears as the scaling parameter, while the constant a is a van der Waals-type coefficient that accounts for the extended volume effect. In this work, its value is taken to be 1.4.

The model (1) in quasi-linear form is written as below:

$$\frac{\partial \mathscr{U}}{\partial t} + \frac{\partial F(\mathscr{U})}{\partial x} = 0,\ -\infty < x < \infty,\ t \geq 0. \tag{2}$$

With the vectors of conserved variables and corresponding flux given by

$$\mathscr{U} = \begin{pmatrix} \rho \\ \rho q \\ \rho u \end{pmatrix} \text{ and } \mathrm{F}(\mathscr{U}) = \begin{pmatrix} \rho u \\ \rho q u \\ \rho u^2 + p + q \end{pmatrix}. \tag{3}$$

The characteristic field analysis in [10] is given by using the vector $\mathscr{V}$ of state variables ρ, q, and u. A new system of equations is obtained by converting the model in equation (1) writen below:

$$\frac{\partial \mathscr{V}}{\partial t} + \mathbf{A}(\mathscr{V}) \frac{\partial \mathscr{V}}{\partial x} = 0, \tag{4}$$

with

$$\mathbf{A}(\mathscr{V}) = \begin{pmatrix} u & 0 & \rho \\ 0 & u & 0 \\ \dfrac{A\gamma\rho^{\gamma-2}}{(1-a\rho)^{\gamma+1}} & \dfrac{1}{\rho} & u \end{pmatrix}. \tag{5}$$

Solving the characteristic equation $\det(\mathbf{A} - \lambda\mathbf{I}) = 0$ for 3×3 Identity matrix $\mathbf{I}$ gives the following set of eigenvalues:

$$\lambda_1 = u - \sigma, \lambda_2 = u \text{ and } \lambda_3 = u + \sigma, \tag{6}$$

where $\sigma = \sqrt{\dfrac{A\gamma\rho^{\gamma-1}}{(1-a\rho)^{\gamma+1}}} > 0$ since $1 \gg a\rho \geq 0$. The corresponding right eigenvectors are given as:

$$R_{(1)} = \begin{pmatrix} -\rho \\ 0 \\ \sigma \end{pmatrix},\ R_{(2)} = \begin{pmatrix} 1 \\ -\sigma^2 \\ 0 \end{pmatrix},\ R_{(3)} = \begin{pmatrix} \rho \\ 0 \\ \sigma \end{pmatrix}. \tag{7}$$

Under the conditions of density positivity and the real-valued term σ, it is concluded that the eigenvalues are real and distinct, resulting in a strictly hyperbolic system of conservation laws.

Consider the quantity $\nabla\lambda_i \cdot R_{(i)}$ computed for each $i = 1, 2, 3$. For $i = 1$ and 3, this quantity is non-zero. Hence, 1- and 3-characteristic fields are genuinely nonlinear. The middle one is linearly degenerate because $\nabla\lambda_2 \cdot R_{(2)} = 0$.

Next, the Riemann invariants are derived by solving the equations, $\dfrac{d\rho}{r_i{}^1} = \dfrac{dq}{r_i^2} = \dfrac{du}{r_i^3}$ for the i^{th} component of the corresponding right eigenvector of the associated characteristic field. The Table 1 below gives these relations.

Table 1. Characteristic fields and Riemann invariants

Characteristics field No.	Riemann invariants	
1-Characteristic field	$\Upsilon_1^1 = q$	$\Upsilon_2^1 = u + \int \frac{\sigma(\xi)}{\xi} d\xi$
2-Charteristic field	$\Upsilon_1^2 = u$	$\Upsilon_2^2 = q + p$
3-Characteristic field	$\Upsilon_1^3 = q$	$u - \int \frac{\sigma(\xi)}{\xi} d\xi$

The initial discontinuous data is given for the vector of primitive variables as $\mathscr{V}_l = (\rho_l, q_l, u_l)^{tr}$ and $\mathscr{V}_r = (\rho_r, q_r, \sqcap_r)^{tr}$ where the subscripts l and r denote the left and right states for some fixed x (usually the middle value of the spatial domain). The model coupled with this type of initial data admits a weak solution with four different regions. These four regions are denoted as

$$\mathscr{V}_l = (\rho_l, q_l, u_l)^{tr}, \quad \mathscr{V}_- = (\rho_-, q_-, u_-)^{tr}, \quad \mathscr{V}_+ = (\rho_+, q_+, u_+)^{tr}, \quad \mathscr{V}_r = (\rho_r, q_r, \sqcap_r)^{tr}. \tag{8}$$

It is well known that the linearly degenerate middle field represents a contact discontinuity wave, and the first and third represent either shock or rarefaction waves. Section 3 is devoted to these waves' fundamental properties and essential relationships.

3. Exact Riemann solution

The 1-characteristic field is genuinely linear and gives rise to either a shock or a rarefaction wave. First, consider the case of a shock wave. In this case, the left and right regions inside the solution are separated by the middle region in such a way that the potential remains constant bu$t$ density increases and velocity decreases from left to right-hand side, i.e., $q_l = q_-$, $\rho_l < \rho_-$ and $u_l > u_-$.

The calculations presented in [10] are not repeated in detail here. Only the formula for shock speed S_1 velocity u_- are presented here. Referring to Figure 1, a shock wave is a discontinuous wave separating two states, depicted in red.

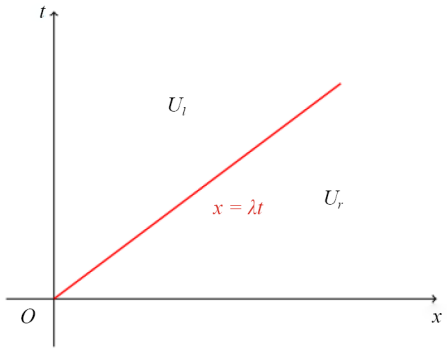

Figure 1. A layout for a shock wave

The speed of this shock wave is written as:

$$S_1 = u_l - \sqrt{\frac{A\rho_-}{\rho_l(\rho_- - \rho_l)}\left[\left(\frac{\rho_-}{1-a\rho_-}\right)^\gamma - \left(\frac{\rho_l}{1-a\rho_l}\right)^\gamma\right]}. \tag{9}$$

The potential remains constant across the shock, and the following relation gives the velocity:

$$u_- = \frac{\rho_l u_l}{\rho_-} + \frac{S_1(\rho_- - \rho_l)}{\rho_-}. \tag{10}$$

Similarly, for the 3-characteristic curve, either a rarefaction wave or a shock wave separates the left and right states. In the case of a 3-shock wave, the corresponding shock speed S_3 and velocity u_+ are as follows:

$$S_3 = u_r + \sqrt{\frac{A\rho_+}{\rho_r(\rho_+ - \rho_r)}\left[\left(\frac{\rho_+}{1-a\rho_+}\right)^\gamma - \left(\frac{\rho_r}{1-a\rho_r}\right)^\gamma\right]}, \tag{11}$$

$$u_+ = \frac{\rho_r u_r}{\rho_+} + \frac{S_3(\rho_+ - \rho_r)}{\rho_+}. \tag{12}$$

The other two state variables satisfy the conditions, $q_+ = q_r$, and $\rho_- \geq \rho_r$. In the case of the one-rarefaction wave, which connects smoothly the left and right states, the state variables satisfy the following conditions:

$$q_- = q_l,\ u_- + \int \frac{\sigma(\xi)}{\xi} d\xi = u_l + \int \frac{\sigma(\xi)}{\xi} d\xi,\ \ and\ \rho_l \geq \rho_-. \tag{13}$$

The formula details for state variables inside the rarefaction wave are missing [10]. A rarefaction wave is the self-similar continuous weak solution of the Cauchy problem associated with the system of equations in equation (3). It is shown in Figure 2 as a general case:

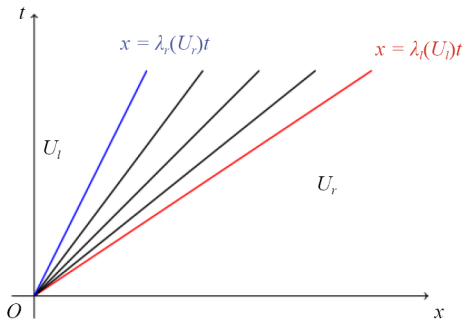

Figure 2. A layout for the rarefaction wave

The slope inside this wave region is given by:

$$\frac{dx}{dt} = \frac{x}{t} = \lambda_{-} = u - \sigma. \tag{14}$$

Hence, the solution inside the rarefaction fan is found by solving the nonlinear system given below:

$$u = \frac{x}{t} + \sigma \text{ and } F(\rho) = u - u_L + \int_{\rho_L}^{\rho} \frac{\sigma}{\rho} d\rho = 0. \tag{15}$$

The one-rarefaction fan has a head and tail, which are shown in red and blue colors. Similarly, the results for the three-rarefaction wave corresponding to the 3-characteristic can be written as follows:

$$q_{+} = q_r,\ u_{+} - \int \frac{\sigma(\xi)}{\xi} d\xi = u_r - \int \frac{\sigma(\xi)}{\xi} d\xi \text{ and } \rho_{+} \leq \rho_r. \tag{16}$$

The velocity and density in the three-rarefaction fan are determined by solving this nonlinear system:

$$u = \frac{x}{t} + \sigma \text{ and } F(\rho) = u - u_R + \int_{\rho}^{\rho_R} \frac{\sigma}{\rho} d\rho = 0. \tag{17}$$

It is evident that to get the solution inside the rarefaction fan or shock speeds, we require ρ_{-} and ρ_{+}. The details are presented in [10]. Here, it is only addressed that these values are the solutions of a nonlinear system, given below:

$$\mathscr{F}\left(\rho_{-},\ \rho_{+},\ \mathscr{V}_l,\ \mathscr{V}_r\right) = 0, \tag{18}$$

$$\mathscr{G}\left(\rho_{-},\ \rho_{+},\ \mathscr{V}_l,\ \mathscr{V}_r\right) = 0, \tag{19}$$

where $\mathscr{F}\left(\rho_{-},\ \rho_{+},\ \mathscr{V}_l,\ \mathscr{V}_r\right) \equiv u_r - u_l + \mathscr{F}_r + \mathscr{F}_l$, with

$$\mathscr{F}_l\left(\rho_{-},\ \mathscr{V}_r\right) = \begin{cases} \sqrt{m_1 \left(\dfrac{\rho_{\_}}{1 - a\rho_{\_}}\right)^{\gamma} + m_2 \dfrac{\rho_{\_}^{\gamma-1}}{\left(1 - a\rho_{\_}\right)^{\gamma}} + \dfrac{m}{\rho_{\_}} + m_4}, & \text{when } \rho_l < \rho_{\_}, \\ \\ \displaystyle\int_{\rho_l}^{\rho_{\_}} \frac{\sigma(\xi)}{\xi} d\xi, & \text{when } \rho_{\_} \leq \rho_l. \end{cases} \tag{20}$$

And

$$\mathscr{F}_l(\rho_-,\ \mathscr{V}_r)=\begin{cases}\sqrt{m_1\left(\dfrac{\rho_-}{1-a\rho_-}\right)^{\gamma}+m_2\dfrac{\rho_-^{\gamma-1}}{(1-a\rho_-)^{\gamma}}+\dfrac{m}{\rho_-}+m_4}, & \text{when } \rho_l<\rho_-,\\ \displaystyle\int_{\rho_l}^{\rho_-}\frac{\sigma(\xi)}{\xi}d\xi, & \text{when } \rho_-\le\rho_l.\end{cases} \tag{21}$$

The second nonlinear equation comes from $\mathscr{G}(\rho_-,\ \rho_+,\ \mathscr{V}_l,\ \mathscr{V}_r)\equiv\mathscr{G}_r-\mathscr{G}_l$ where

$$\mathscr{G}_l(\rho_-,\ \mathscr{V}_l)=A\left(\frac{\rho}{1-\bar{a}\rho_-}\right)^{\gamma}+q_l. \tag{22}$$

And

$$\mathscr{G}_r(\rho_+,\ \mathscr{V}_r)=A\left(\frac{\rho_+}{1-a\rho_+}\right)^{\gamma}+q_r. \tag{23}$$

The 2-characteristic field is linearly degenerate and gives rise to a contact wave. The characteristic condition for the contact wave is:

$$\lambda_2(\mathscr{V}_-)=S_2=\lambda_2(\mathscr{V}_+). \tag{24}$$

This results $u_-=u_+=S_2$. Finally, it is necessary to state that the situation in which eigenvalues coincide is impossible unless $\sigma=0$. The possible wave configuration can be any one of the following:

1. One-shock, two-contact discontinuity, and three-rarefaction;
2. One-shock, two-contact discontinuity, and three-shock;
3. One-rarefaction, two-contact discontinuity, and three-rarefaction;
4. One-rarefaction, two-contact discontinuity, and three-shock.

The wave structure for the first case is demonstrated in Figure 3.

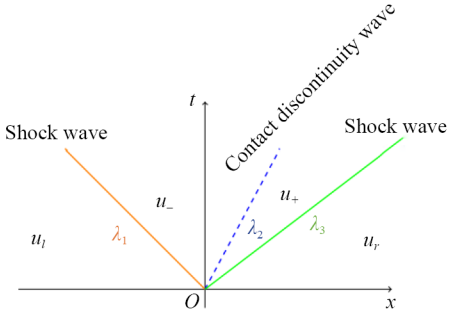

Figure 3. The Riemann solution structure

The following steps formulate the process of getting an exact solution:

1. Compute the eigenvalues.
2. Select the wave type and its corresponding wave speed (for shock waves) or head speed (for rarefaction waves).
3. Solve for unknown quantities by equations (18) and (19).

Sample the solution for general values of x and t.

It completes the required details to get the exact solution to the Riemann problem associated with the Cargo Leroux model.

4. Godunov method

Godunov's method is the primary approach for solving hyperbolic systems of partial differential equations. It is also an essential method for numerically investigating complex phenomena, including compressible flows, thermonuclear processes, and detonation processes, as referenced in [21–29].

Although it is based on standard finite volume discretization, the principle of flux calculation with the exact solution of the corresponding Riemann problem is the distinctive feature of this method. The errors are significantly less than numerical methods like finite difference, central schemes, and Roe solvers. This section presents the Godunov scheme for the considered model.

The space and time steps are denoted by Δx and Δt, respectively. After discretization of the spatial domain into cells, the interface of the j^{th} and the $j+1$ cells are denoted by $x_{j+1/2} = (j+1/2)\Delta x,\ j \in \mathbb{Z}$.

The discrete initial values are obtained as cell averages given by

$$U_j^0 = \frac{1}{\Delta x}\int_{x_{j-1/2}}^{x_{j+1/2}} U_0(x)dx. \tag{25}$$

Knowing the Riemann solution $U(x,\ t)$ gives the piecewise constant solution U_j^n over the grid cells at each time step, which can be used to get the updated solution U_j^{n+1} in time. This update is performed using the exact solution of the Riemann problem at each cell face. The method takes the following steps:

$$U_j^{n+1} = U_j^n - \frac{\Delta t}{\Delta x}\left(F\left(U\left(0-;\ U_j^n,\ U_{j+1}^n\right)\right) - F\left(U\left(0+;\ U_{j-1}^n,\ U_j^n\right)\right)\right). \tag{26}$$

With the condition on the maximum time step given as:

$$\frac{\Delta t}{\Delta x}\max\left\{\left|\lambda_k\left(U_j^n\right)\right|,\ k=1,\ 2,\ 3\right\} \leqslant \frac{1}{2}. \tag{27}$$

The time-step is bounded to ensure that waves from adjacent cells do not cross each other. At each time step of the finite volume method, a local Riemann problem is solved for the exact solution based on the density values obtained by solving a nonlinear system of equations (18) and (19) at each time level. The exact solution differs from the numerical solution in the context of a time-stepping algorithm. The numerical solution is obtained using a time-step finite volume method; however, the exact solution gives the values after some time T. In this view, although the Newton-Raphson method is used to obtain the exact solution, it is usual to mention it as an exact solution. The reader is referred to the references stated above for more details. The Newton-Raphson method for a system of nonlinear equations is extremely sensitive to the initial guess values. Hence, finding an appropriate initial guess for the solution of a nonlinear system is crucial. As a result, the residual function is computed at each step and minimized to get the appropriate initial guess. Moreover, it is stated that all the calculations are possible to carry out to get the correct solution by imposing checks for

positivity of the density ρ and the quantity $1 - a\rho$. Lastly, the initial data is provided for the state variables vector V, and the scheme updates the conserved variables vector U. Therefore, at each iteration, a conversion from the primitive to the conserved variables and vice versa is also required. The flow chart below (Figure 4) is presented as a visual representation of the process.

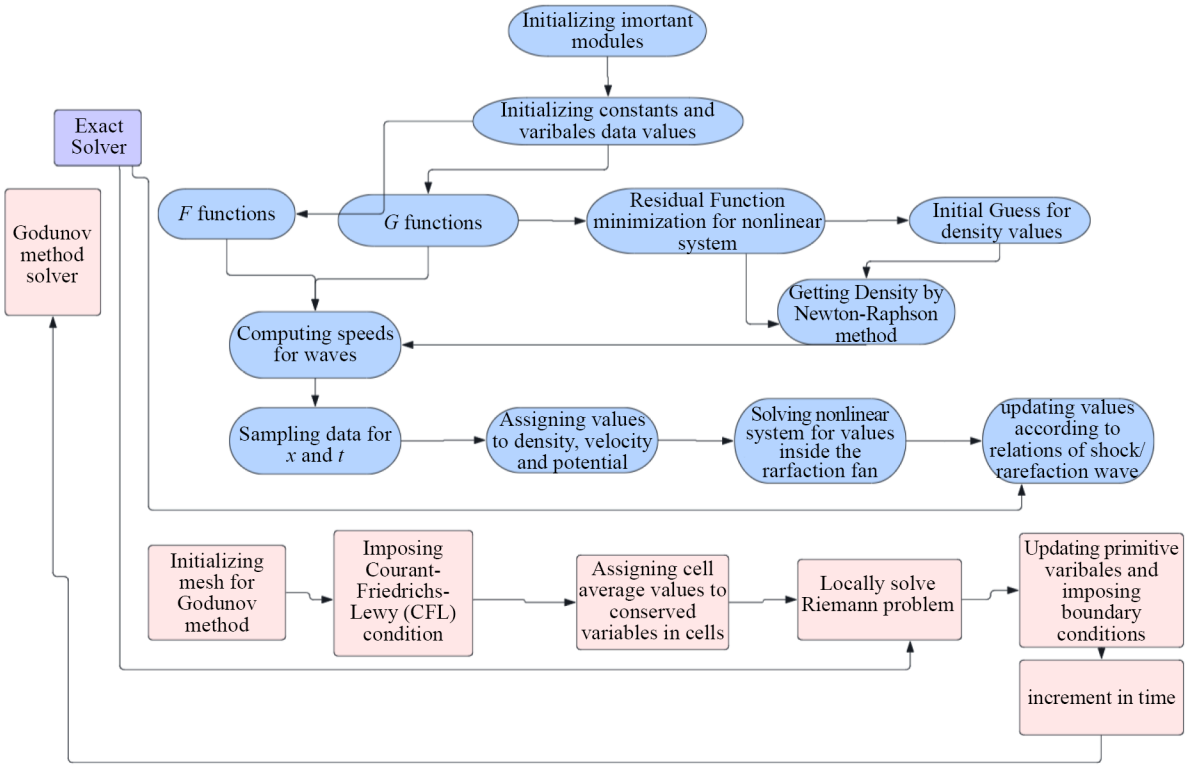

Figure 4. Flow chart of computations

5. Numerical results

This section presents the numerical test cases from the reference article [10]. The numerical results are compared with the exact solution for cases I and II. These two test cases have been simulated because of different wave structures. The first test case represents a combination of shock and rarefaction waves, and the second test case demonstrates the solution composed of two shocks. The parameters A, a, γ are the same for both test cases. The final time is different for each test case and is fixed according to the results of the reference article. The zero-gradient boundary conditions are chosen for the numerical setup. This ensures that solutions near the boundary continue smoothly without reflecting anything artificially.

Test 1: The initial data values used for this problem are given below:

$$V(x,\,0) \;=\; \begin{cases} \mathscr{V}_l = (5.99924,\; 2.7996,\; 0.5975)^{tr}, & x < 0 \\ \\ \mathscr{V}_r = (7.99242,\; 1.37452,\; -6.19633)^{tr}, & x > 0. \end{cases} \tag{28}$$

The values for ρ_- and ρ_+ are 18.8009 and 18.450, respectively. Hence, according to the discussion in section 3, the solution comprises four regions, separated by a one-shock wave, a two-contact discontinuity, and a three-shock wave. Numerical solutions yield similar solution profiles, with only minor differences in the locations of waves, as shown in Figure 5. These results are simulated for a time $t = 0.03$ s, and the value of the constant a is chosen to be 0.035. The one-shock is at $x = -0.18$ while the two is at $x = -0.2$.

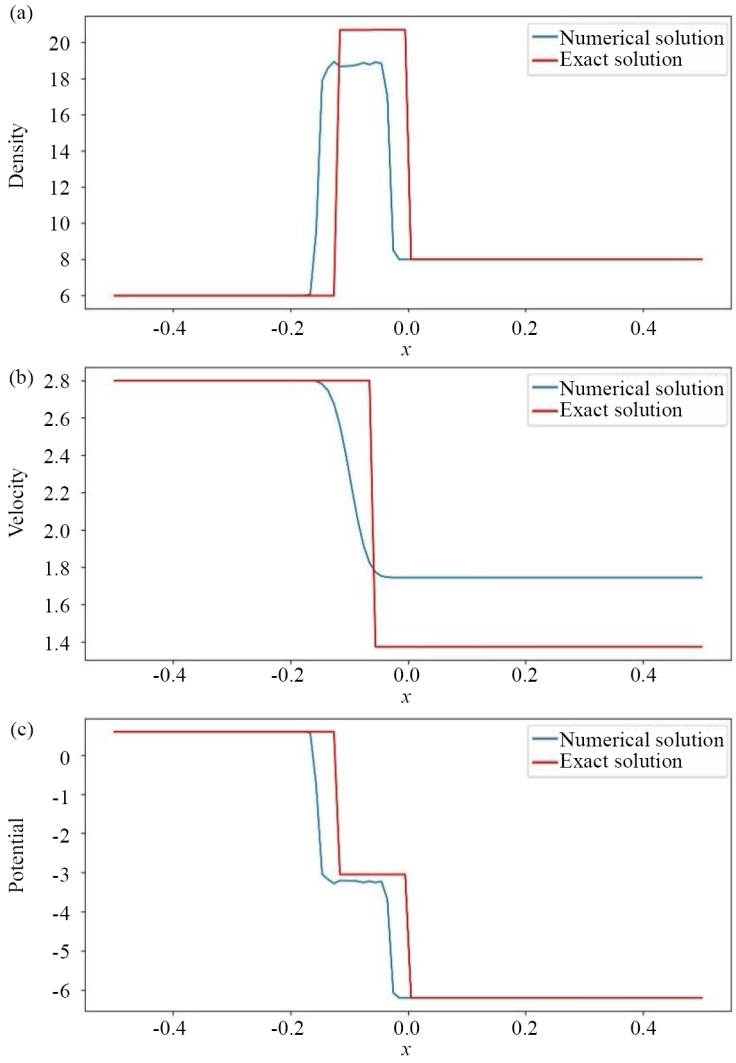

Figure 5. Results for test 1 at time $t = 0.03$ and step size $\Delta x = 0.001$

Test 2: The initial data values used for this problem are given below:

$$\mathscr{V}(x,\,0) = \begin{cases} \mathscr{V}_l = (0.96,\,0.1379,\,1.0833)^{tr}, & x < 0 \\ \\ \mathscr{V}_r = (1.7741,\,1.5,\,1.1187)^{tr}, & x > 0 \end{cases} \tag{29}$$

The values for ρ_- and ρ_+ are 2.13 and 0.6330, respectively. Hence, according to the discussion in section 3, the solution comprises four regions, separated by a one-shock wave, a two-contact discontinuity, and a three-rarefaction wave and a three-rarefaction wave as shown in Figure 6. The rarefaction wave's head and tail locations are at $x = 0.45$ and $x = 0.22$, respectively, with the head's speed of 2.1320. The one-shock is located at $x = -0.94$.

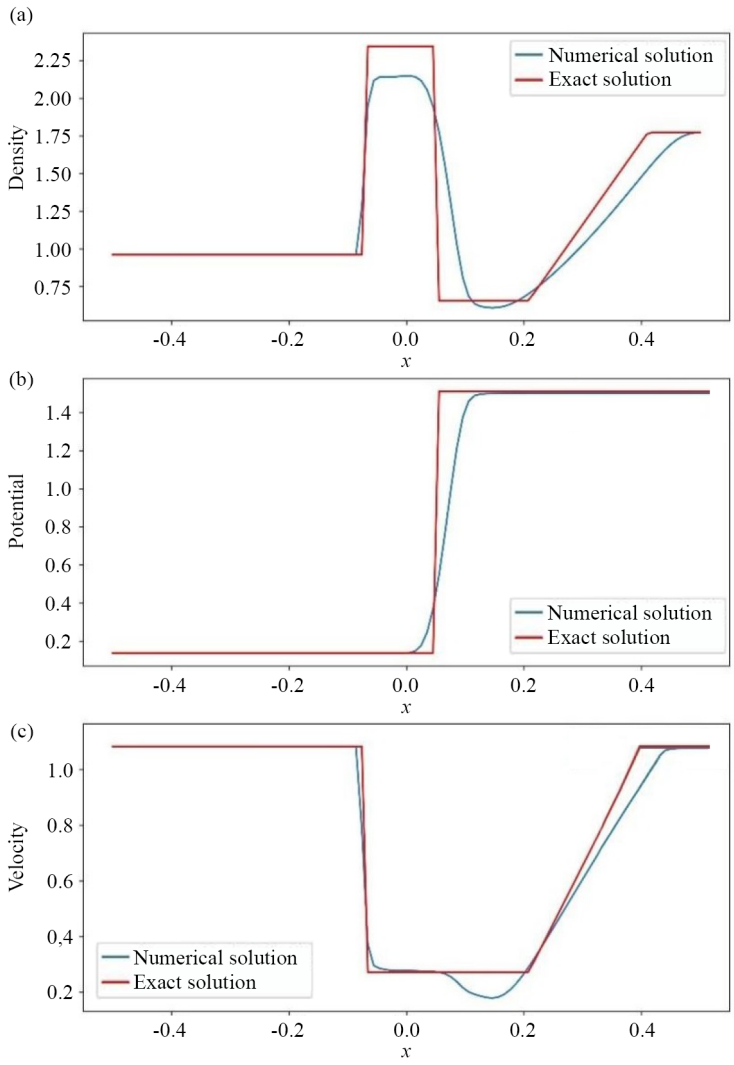

Figure 6. Results for test 2 at time $t = 0.2$ and step size $\Delta x = 0.001$

6. Conclusions

The Godunov method has been used to simulate the Riemann problem for the Cargo LeRoux model numerically. This work revisits the exact solution of the model and fills essential gaps in describing the whole solution. Numerical difficulties have been identified that must be addressed to obtain stable numerical solutions. Two test cases have been presented to compare the exact Riemann and numerical solutions. The initial data consists of constant data, comprising two sets of values related to the spatial position $x = 0$. The spatial domain ranges from $x = -0.5$ to $x = 0.5$, whereas the final time varies for the cases considered in the reference article [12].

Further improvements will focus on achieving higher accuracy and reducing oscillations in numerical solutions. It is worth noting that the same model has been simulated using the central scheme; however, the results are highly oscillatory and therefore not presentable. Another extension of the work is to apply physics-informed neural network methods, as these methods also utilize the exact solution to the Riemann problem.

Acknowledgement

The author Ilyas Khan extends the appreciation to the Deanship of Postgraduate Studies and Scientific Research at Majmaah University for funding this research work through the project number (ER-2025-2118).

Conflict of interest

The authors declare that they have no conflicts of interest.

References

[1] Lax PD. Hyperbolic systems of conservation laws II. *Communications on Pure and Applied Mathematics*. 1957; 10(4): 537-566.
[2] Smoller J. *Shock Waves and Reaction-Diffusion Equations*. 2nd ed. New York: Springer Verlag; 1994.
[3] Toro EF. *Riemann Solvers and Numerical Methods for Fluid Dynamics*. Berlin: Springer-Verlag; 2009.
[4] Sharma VD. *Quasilinear Hyperbolic Systems, Compressible Flows, and Waves*. Boca Raton: CRC Press; 2010.
[5] Zeidan D. Drag force simulation in explosive volcanic flow. *AIP Conference Proceedings*. 2015; 1648: 030007.
[6] Zeidan D, Touma R, Slaouti A. Application of a thermodynamically two-phase flow model to the high-resolution simulation of compressible gas-magma flow. *International Journal for Numerical Methods in Fluids*. 2014; 76: 312.
[7] Kumozec D, Nedeljkov M. The Riemann problem for the generalized Chaplygin gas with a potential. *Zeitschrift für Angewandte Mathematik und Physik*. 2024; 75(2): 67.
[8] Sahoo SM, Sekhar TR, Raja Sekhar GP. Wave interactions in pressureless Cargo-LeRoux model with flux perturbation. *Mathematical Methods in the Applied Sciences*. 2023; 46(8): e9009.
[9] Karna AK, Satapathy P. Lie symmetry analysis for the Cargo-LeRoux model with isentropic perturbation pressure equation of state. *Chaos, Solitons & Fractals*. 2023; 177: 114241.
[10] Sunita J, Sahadeb K. Exact solution of the flux perturbed Riemann problem for Cargo-LeRoux model in a van der Waals gas. *Chaos, Solitons & Fractals*. 2022; 161: 112369.
[11] Nath T, Gupta RK, Singh LP. Solution of Riemann problem for ideal polytropic dusty gas. *Chaos, Solitons & Fractals*. 2017; 95: 102-110.
[12] Kuila S, Raja Sekhar T. Interaction of weak shocks in drift-flux model of compressible two-phase flows. *Chaos, Solitons & Fractals*. 2018; 107: 222-227.
[13] Andrianov N, Warnecke G. On the solution to the Riemann problem for the compressible duct flow. *SIAM Journal on Applied Mathematics*. 2004; 64(3): 878-901.
[14] Giacomazzo B, Rezzolla L. The exact solution of the Riemann problem in relativistic magnetohydrodynamics. *Journal of Fluid Mechanics*. 2006; 562: 223-259.
[15] Pang Y, Ge J, Liu Z, Hu M. The Riemann problem for one-dimensional isentropic flow of a mixture of a non-ideal gas with small solid particles. *Results in Physics*. 2019; 15: 102587.
[16] Li J. Note on the compressible euler equations with zero temperature. *Applied Mathematics Letters*. 2001; 14(4): 519-523.
[17] Chen G, Liu H. Formation of δ-shocks and vacuum states in the vanishing pressure limit of the solutions to the Euler equations for isentropic fluids. *SIAM Journal on Mathematical Analysis*. 2003; 34(4): 925-938.
[18] Chen G, Liu H. Concentration and cavitation in the vanishing pressure limit of solutions to the Euler equations for non-isentropic fluids. *Physica D: Nonlinear Phenomena*. 2004; 189: 141-165.

[19] Jin Y, Qu A, Yuan H. Radon measure solutions to Riemann problems for isentropic compressible Euler equations of polytropic gases. *Communications in Applied Mathematics and Computation*. 2022; 5(3): 1097-1129.

[20] Kipgen L, Randheer S. δ-shocks and vacuum states in the Riemann problem for isothermal van der Waals dusty gas under the flux approximations. *Physics of Fluids*. 2023; 35(1): 016116.

[21] Isaacson E, Temple B. Convergence of the 2×2 Godunov method for a general resonant nonlinear balance law. *SIAM Journal on Applied Mathematics*. 1995; 55(3): 625-640.

[22] Chinnayya A, LeRoux AY, Seguin N. A well-balanced numerical scheme for the approximation of the shallow-water equations with topography: The resonance phenomenon. *International Journal of Finite*. 2004; 1(1): 33.

[23] LeFloch PG, Thanh MD. A Godunov-type method for the shallow water equations with discontinuous topography in the resonant regime. *Journal of Computational Physics*. 2011; 230(20): 7631-7660.

[24] Ambroso A, Chalons C, Raviart PA. A Godunov-type method for the seven-equation model of compressible two-phase flow. *Computers & Fluids*. 2012; 54: 67-91.

[25] Saurel R, Abgrall R. A multiphase Godunov method for compressible multifluid and multiphase flows. *Journal of Computational Physics*. 1999; 150(2): 425-467.

[26] Schwendeman DW, Wahle CW, Kapila AK. The Riemann problem and a high-resolution Godunov method for a model of compressible two-phase flow. *Journal of Computational Physics*. 2006; 212(2): 490-526.

[27] Zhou L, Chen QX, Li YJ, Feng RL, Xue ZJ. Godunov-type scheme for air-water transient pipe flow considering variable heat transfer and laboratorial validation. *Engineering Applications of Computational Fluid Mechanics*. 2024; 18(1): 2370931.

[28] Igor K, Dmitry K. The WENO reconstruction in the Godunov method for modeling hydrodynamic flows with shock waves. *Journal of Physics: Conference Series*. 2021; 2028(1): 012023.

[29] Hu M, Wang G, Liu G, Peng Q. The application of Godunov SPH in the simulation of energetic materials. *International Journal of Computational Methods*. 2020; 17(7): 1950028.